JCTC Journal of Chemical Theory and Computation

Article

pubs.acs.org/JCTC

Tuning Electron Transport through Functionalized $C_{20}H_{10}$ Molecular Junctions

Laura Zoppi,[†] Andrea Ferretti,[‡] and Kim K. Baldridge*[,†]

[†]Department of Chemistry, University of Zürich, Winterthurerstrasse 190, CH-8057 Zürich, Switzerland

[‡]Centro S3, CNR-Instituto Nanoscienze, via Campi 213/A, 41125 Modena, Italy

Supporting Information

ABSTRACT: First-principles methodology based on density functional theory (DFT) is used to investigate charge transport phenomena in molecular junctions, with the central active molecular element based on corannulene, $C_{20}H_{10}$, assembled between two carbon nanotubes (CNT). A number of key factors associated with the design of the molecular nanojunction are shown to have an impact on electron transport to varying degrees, including (I) the composition of the spacer linking the leads to the active element, (II) the composition of the active molecule element, (III) the sensor capabilities of the active element, and (IV) the response of the junction to an external electric field. This study demonstrates the ability to integrate molecular electronic functionality into electronic nanocircuits and provides novel insight into the design of new types of molecular-based devices by revealing the relationship between charge transport mechanisms and the electronic structure of molecular junction components.

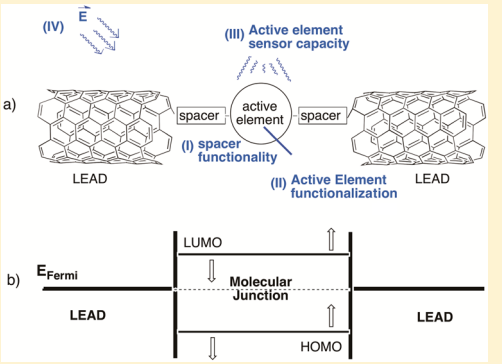

INTRODUCTION

There is renewed interest in the use of π-conjugated molecules as components in nanoscale electronics and optoelectronic devices,[1−4] particularly in view of recent abilities to construct single-molecule junctions and measure their transport properties.[4−6] As conductor dimensions approach the nanoscale, design principles turn toward creating molecules with tunable functionality to enable control of charge transport on the molecular scale.[3,4] Despite being able to control molecular design through chemical synthesis, the ability to guide the conductance of individual molecules by external means is still a formidable challenge. There remain a number of factors that cannot be controlled in experiments, causing measured conductance to vary significantly.[3,7] In such a complex scenario, the detailed investigation of single molecules connected to macroscopic electrodes provides a powerful template for improving our knowledge of electronic transport phenomena in molecular junctions, which, in turn, should lead to advancements in experimental measurement capabilities as well as in the fundamental theoretical understanding of their construction.[7]

From this perspective, the extended family of curved aromatics based on the smallest bowl-shaped fullerene fragment, corannulene, $C_{20}H_{10}$ (**1**),[8] are key targets of interest for applications in molecular electronics, enabling focused design and tuning of a variety of molecular building blocks with tailored electronic properties.[9] The local curvature of the parent molecule, which manifests a substantial dipole of 2.1 D,[10] can be modified via chemical functionalization, providing an avenue to fine-tune select properties such as transport/optical gap and polarizability.[11,12]

The key to unlocking the electronic properties of such molecular fragments for practical applications lies in the solid-state packing and intermolecular interactions of the individual curved aromatic bowl structures. Assembled in the solid state, these molecular bowls can be exploited as junction materials for transport processes in various complex environments, such as active organic layers in optoelectronic interfaces,[9,11,13] molecular monolayers supported on metallic surfaces,[14] or single molecules in molecular junctions.[12] As such, these molecular bowl-shaped fragments provide a consistent platform of materials ideal for advancing our understanding of fundamental transport processes in molecular junctions with tailored properties.

In this work, a first-principle methodology based on density functional theory (DFT) is used to investigate charge transport phenomenon in molecular junctions designed with a functionalized corannulene unit, *f*-$C_{20}H_{10}$, as the main active molecular element. The functionalized corannulene is assembled between two carbon nanotube (CNT) components that serve as the leads. The use of CNTs as electrode materials has been shown recently to serve as suitable electric contacts at junctions, enabling improved control of the geometry at the interface over that with metal electrodes.[15,16] The effect of different design factors is investigated with regard to modulation of electron transport through the CNT−[spacer]−*f*-$C_{20}H_{10}$−[spacer]−

Received: June 24, 2015

DOI: 10.1021/acs.jctc.5b00592
J. Chem. Theory Comput. XXXX, XXX, XXX−XXX

CNT junctions (Figure 1, junction features), including (I) the composition of the spacer linking the leads to the active element, (II) the composition of the active molecule element, (III) the sensor capabilities of the active element, and (IV) the response of the nanojunction to an external electric field.

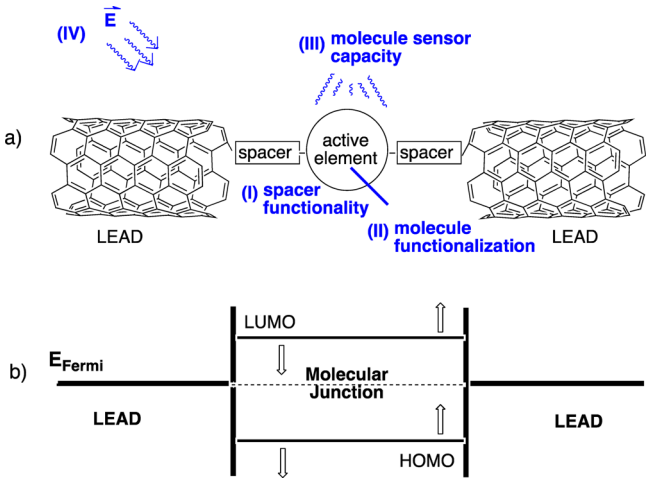

Figure 1. (a) Factors affecting transport properties through a molecular junction: (I) chemical composition of the linking-spacer, (II) chemical functionalization of the active element, (III) chemical reactions occurring at the surface of the active element, and (IV) application of an external field. (b) Implications of the junction features on the alignment of the active element's HOMO and LUMO levels with respect to the Fermi level of the leads.

THEORETICAL METHODOLOGY AND DESIGN APPROACH

Nanojunction Design. Representation of a molecular nanojunction in terms of its basic components enables the junction features responsible for control of conductance through the junction to be considered (Figure 1). Such features can be partitioned into those related to (a) chemical composition of molecular components of the designed nanojunction and (b) external elements, such as electric field effects or target molecules that interact with the nanojunction through the active element.

Chemical Composition. Key chemical composition features of the nanojunction that are fundamental to the control of transport through the junction include the structure and composition of the (a) lead components, (b) spacer linker components to the leads, and (c) the central molecular component. In the present study, the electrode component is an armchair, metallic (5,5)-CNT. The use of nanostructured materials as leads creates a large surface area that has the potential to enhance the efficiency and performance of the device. However, significantly more testing is needed to understand the details of nanojunctions made with nanostructured materials. The chemical composition of the linking spacer of the junction (Figure 1a, (I)) functions either to inhibit transport, largely decoupling the electronic interaction between molecule and leads due to disruption of π-electron delocalization, or to facilitate transport, by preserving π-electron delocalization through the junction. The ability to rationally design substituted forms (Figure 1a, (II)) enables one to tailor energy level alignments at the molecule−electrode interface (Figure 1b),[7,17] contributing to a further modulation in electron transport through the junction.

External Elements. The possibility of performing chemical reactions on the surface of the active element in the junction also constitutes a means toward controlling electron transport through the junction (Figure 1a, (III)). Moreover, such investigations lend themselves toward the design of nanosensing systems[18] for the detection of target molecules interacting with the molecular unit within the junction.

Depending on the nature of the central active element of the junction, one may consider electron transport under the influence of an electric field. An active component with a significant multipole moment can be exploited to govern the molecular orientation of the active element inside the nanojunction under the influence of an electrical stimulus (Figure 1a, (IV)).[12] Such characteristic features have the potential to manifest a molecular nanojunction with interesting field-oriented materials properties.[10]

Current Design. To explore fundamental electronic transport properties under a variety of conditions, a series of nanojunction systems based on corannulene as the active element has been investigated. The key component of corannulene is its characteristic curved morphology, which can be modulated with functionalization. Rationally designed functionalization enables the control of energy level alignments at the molecule−electrode interface. The resulting morphology changes in curvature with functionalization, in turn, modulate the inherently large intrinsic dipole of the parent corannulene, which governs molecular orientation under electrical stimulus when assembled into a molecular junction.[12] Due to the relatively large surface area of the cap of corannulene, there is also the possibility of investigating the sensitivity of transport properties as a function of target molecules interacting with the bowl surface in the junction.

Electronic Structure. First-principles techniques within the framework of density functional theory (DFT) were employed to investigate structural and electronic properties of the designed molecular junctions based on functionalized $C_{20}H_{10}$ connected to (5,5)-CNT leads with varying molecular spacers as linkers. The structure of the targeted, functionalized $C_{20}H_{10}$ molecules used as active elements in the junctions was initially fully optimized with the PBE density functional[19] in combination with the Def2-TZVPP basis set[20] using standard quantum chemical techniques, as implemented in the GAMESS software package.[21] All optimized geometries were uniquely characterized via second-derivative (Hessian) analysis.

The fully optimized molecular structures were then linked to the CNT leads in order to build the junction. To mimic a semi-infinite CNT lead, the assembled molecular junctions were optimized within a supercell/plane-wave approach (Quantum ESPRESSO package[22]) at the PBE level, using periodic boundary conditions and Vanderbilt ultrasoft pseudopotentials.[23] A supercell of ~17 repeated CNT units (≈43.1 Å) was used for all molecular junctions, including 13.5 Å of lateral separation between images to avoid spurious replica interaction. The single-particle electronic wave functions (charge densities) were expanded in a plane-wave basis set, up to an energy cutoff of 25 Ry (250 Ry). For Brillouin zone integration, a (114) k-point sampling was used (although it is not strictly required, the use of k-points along the transport direction is practical when computing transport properties using the WanT software[24,25]). During relaxation, force components were converged to within 5×10^{-4} Ry/Bohr, corresponding to 0.013 eV/Å.

DOI: 10.1021/acs.jctc.5b00592
J. Chem. Theory Comput. XXXX, XXX, XXX−XXX

Quantum Conductance. To investigate electron transport through molecular junctions, a standard single-particle Green's function method[26] was adopted, which combines the Landauer approach[27,28] with *ab initio* density functional theory. The infinitely extended nanojunction system is divided into three components, including left lead, right lead, and conductor region (Figure 2). The conductor region contains the molecule,

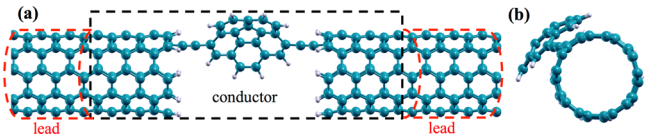

Figure 2. (a) Prototype junction geometry consisting of 1,6-diethynylcorannulene linked to (5,5)-CNT leads in the relaxed configuration: the conductor region includes the molecule and a portion of the leads; the lead regions are highlighted. (b) Side view of the relaxed configuration.

the linker, and a portion of the CNT large enough to accommodate the molecule−CNT interaction. The coherent transport properties of all molecular junctions are evaluated using the Landauer approach,[27−29] which relates the quantum conductance, G, of the junction to its electronic scattering properties through the expression

$$G = \frac{2e^2}{h} T(E_F) \tag{1}$$

where $T(E_F)$ is the transmittance at the Fermi energy E_F. The quantum transmittance can be simply expressed as the trace of a matrix product, using the Fisher−Lee expression[30]

$$T = Tr(\Gamma_L G_C^r \Gamma_R G_C^a) \tag{2}$$

where $G_C^{r,a}$ are the retarded and advanced lattice Green's functions of the conductor region, respectively, and $\Gamma_{(L,R)}$ represent the coupling between the conductor and the leads.[26] In the zero-bias and zero-temperature regime, the transmittance spectra is evaluated using the WanT software,[24] initialized from the ground-state electronic structure as computed by the Quantum ESPRESSO suite.[22] Since a localized basis set is required in the implementation of the theory described above, we follow the approach recently proposed by Agapito et al.[28] and use pseudoatomic orbitals to describe the electronic structure of the leads and conductor subsystems. Upon self-consistency, the matrix elements of the Kohn−Sham Hamiltonian on the pseudoatomic orbitals, φ_i, are computed as

$$H_{i,j} = \sum_n^M \langle \phi_i | \psi_n \rangle \varepsilon_n \langle \psi_n | \phi_j \rangle + \Delta \langle \phi_i | (I - \sum_n^M |\psi_n\rangle\langle\psi_n|) | \phi_j \rangle \tag{3}$$

where ψ_n are the KS eigenvectors (written on the plane-wave basis) and ε_n are their corresponding eigenvalues. As discussed in ref 28, here the sums are limited to M bands (those having a projectability on the pseudoatomic orbitals larger than a given threshold), whereas unrepresentable eigenvectors are shifted by Δ out of the energy region of interest.

In the present calculations, a single-ζ basis (one radial part per angular momentum channel) is used. Since the self-consistent calculations are performed using the plane-wave basis, the approach is shown to be quite accurate given the relative simplicity of the procedure. Specifically, this basis has been tested and found to reproduce well the plane-wave electronic structure in the energy range of interest (up to a few electron volts around the Fermi level of the nanojunction; see Supporting Information). The filtering and shifting parameters governing the accuracy of the basis[28] are set to 0.9 and 5.0 eV, respectively.

RESULTS AND DISCUSSION

Prototype Junction: Electronic Structure and Related Charge Transport Mechanism. The CNT−[spacer]−molecule−[spacer]−CNT junction model investigated in this work consists of $C_{20}H_{10}$-derived molecule linked on each side to a semi-infinite (5,5)-CNT electrode with a specified linker spacer. To construct the junction, a segment of the pristine (5,5)-CNT, closely corresponding to the length of the molecule (about 4 tube units), is removed to create the gap that accommodates the molecular unit (Figure 2).

The description of an infinite electrode (Figure 3a) is achieved by considering a periodically repeated (5,5)-CNT

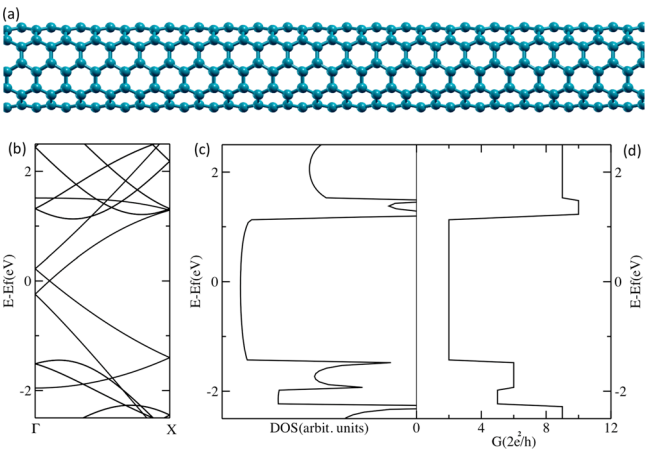

Figure 3. (a) Layer structure of a (5,5) pristine CNT. (b) Energy bands, (d) DOS, and (c) quantum transmittance of the minimal (5,5)-CNT unit cell.

structure with a primitive unit cell consisting of three repeated units along the tube's axis (7.43 Å). The energy bands, density of states (DOS), and electronic conductance of the minimal (5,5)-CNT structure are shown in Figure 3b−d, respectively. The conductance of the ideal (5,5)-nanotube system (Figure 3d) shows the typical step-like shape expected for pristine periodic systems and metallic behavior, which is the result of the high curvature (small radius) of the nanotube. The choice of a (5,5)-CNT as a prototype lead offers the possibility of having a metallic electrode with a moderate diameter (0.69 nm) and a flat transmittance in the energy interval [−1.4, 1.1] eV around the Fermi level, which is ideal for a theoretical study. The quantitative agreement between the electronic structure, in terms of band offsets and band widths (Figure 3b,c), and the quantum conductance (Figure 3d) indicates that this minimal cell size allows for a good representation of the infinite lead within the nearest-neighbor principal layer approximation[28] adopted to perform transport calculations.

For an illustration of a prototypical CNT−[spacer]−molecule−[spacer]−CNT junction, the case of CNT−[1-ethynyl]−$C_{20}H_{10}$−[6-ethynyl]−CNT was investigated, which can be considered to be a $C_{20}H_{10}$-active element linked to a (5,5)-CNT tube through carbon−carbon triple bond linkers.

DOI: 10.1021/acs.jctc.5b00592
J. Chem. Theory Comput. XXXX, XXX, XXX−XXX

The fully relaxed configuration of this junction is shown in Figure 2. The cylindrical symmetry of the acetylene groups serving as spacer units imparts flexibility inside the junction and facilitates π delocalization through the junction.

To gauge the degree of interaction of the molecular orbitals of the active element inside the junction, a comparison of the 1,6-diethynylcorannulene PDOS in the CNT−[1-ethynyl]−$C_{20}H_{10}$−[6-ethynyl]−CNT complex with the DOS of the isolated active element is considered (Figure 4a). Here, the

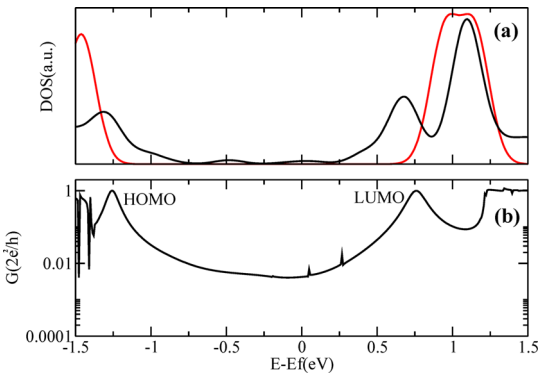

Figure 4. (a) DOS (red curve) of the gas-phase molecule and PDOS (black curve) of the molecule inside the junction. (b) Quantum transmittance in the junction (in units of G_0, the quantum of conductance).

PDOS of the active element in the junction (black) shows broader structures for HOMO and LUMO with respect to the sharp molecular states found for the isolated molecule (red), with the molecular LUMO displaying a multipeak structure. The left-most peak of the LUMO structure in the PDOS is closer to the Fermi energy by ∼0.4 eV than was the pristine isolated molecular LUMO (Figure 4a). The relative position of the frontier molecular orbitals and the Fermi level indicates that transport would be primarily mediated by the LUMO orbital for this junction.

The HOMO and LUMO signatures of the molecular unit inside the junction can be also detected by considering the plot of the quantum conductance versus energy, as shown in Figure 4b. In this specific case, there are two main peaks appearing below the Fermi energy, −1.25 eV, and above the Fermi energy, 0.65 eV, which are aligned with the corresponding HOMO and LUMO peaks in the PDOS plot.

Chemically Tuned Molecular Junctions: Effect of Linker Spacer. The anchoring groups used for linking the molecule to the left and right leads are important components for controlling the properties of molecular junctions. These groups ultimately determine the molecule−electrode coupling strength as well as influence the molecular conformation inside the junction.[7] The nature of the hybridization link from the lead through the junction will influence the extent of π-conjugation, thereby impacting the quantum conductance. As illustrated in the simple case of a biphenyl molecule connected to metal electrodes, one can estimate a modulation in conductance in accord with the square of the π overlap.[3]

Here, the effect of different hybridized anchoring groups (sp/sp^2/sp^3) on electron transport through the CNT−[spacer]−$C_{20}H_{10}$−[spacer]−CNT complex nanojunction is investigated. This analysis has been achieved by inserting a spacer with a CC triple bond (sp), a CC double bond (sp^2), or a CC single bond (sp^3) between the molecule and the CNT leads. Each of the corresponding relaxed geometries in the junction is shown in Figure 5a−c, respectively.

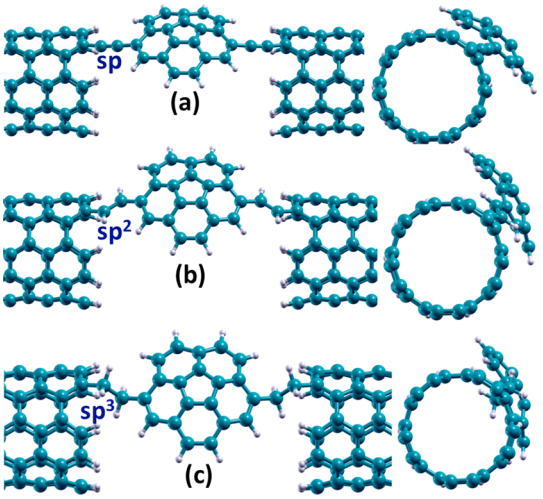

Figure 5. Relaxed structures of the molecular junctions (front and side views) with different linking spacers: (a) sp-hybridized linker spacer, (b) sp^2-hybridized linker spacer, and (c) sp^3-hybridized linker spacer.

In terms of conformation alone, one finds only small differences between the sp- and sp^2-hybridized linkers, with the final orientation of both having the $C_{20}H_{10}$ molecular surface aligned with the tube's mantel. For the latter junction (sp^2), the molecule + linker is turned slightly more out of alignment to better accommodate the hydrogens of the −HC═CH− group. From the perspective of the charge transport properties, one sees only slight modulation in quantum conductance from sp- to sp^2-hybridized linkers, as shown in Figure 6. The two quantum conductance curves are nearly superimposed, with that of the sp^2-hybridized linker being slightly higher through the entire energy range (the ratio close to the Fermi level is ∼3). The two fundamental peaks close to the Fermi energy undergo a slight shift, indicating a small modulation in coupling with the leads for the sp^2-hybridized linker spacer.

Insertion of completely saturated left and right linkers breaks the π conjugation through the nanojunction, effectively acting as a double barrier and electronically decoupling the molecule from the leads. Such a modulation in the linker spacer affects the quantum conductance in a substantial way, as shown in Figure 6. The molecular nanojunction with the $-CH_2-CH_2-$ linker group shows a general reduction in conductance along the whole energy range, with the overall spectrum being drastically different from that of the other two cases. The conductance curve is quite distorted by the appearance of dips, which is a characteristic feature of backscattering processes

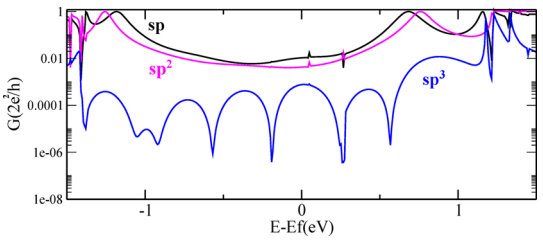

Figure 6. Quantum conductance of the molecular junctions with varying linking spacers: sp/sp^2/sp^3-hybridized groups.

DOI: 10.1021/acs.jctc.5b00592
J. Chem. Theory Comput. XXXX, XXX, XXX−XXX

coming from the presence of an extra double barrier that encloses the conductor region.[31,32] Depending on the incident energy of the carriers, the quantum conductance can either undergo a severe reduction (energy out of resonance with bound states of the well) or a strong enhancement (energy in resonance with bound states of the well), as evidenced by the appearance of peaks in the conductance curve. Similar oscillation patterns have been observed in the backscattering current of a quantum wire attached to noninteracting leads, where the characteristic oscillation behavior could be ascribed to the presence and location details of the double barrier.[32]

Chemically Tuned Molecular Junctions: Effect of Electric Field. The behavior of corannulene-derived bowl fragments under the effect of an electric field becomes particularly important when one is interested in exploiting the response to an electrical stimulus as a means to govern molecular orientation of an active element in a molecular nanojunction.[12] In principle, such a response property would open the possibility of designing efficient molecular switches triggered by an electrical stimulus. Such molecular switchability would require the existence of two isomers that can be controllably converted from one to the other by an electrical stimulus.[17,33−38] In this respect, a fundamental factor in the driving force for switching is the ability to control the direction of the switching response such that the molecular conformation in the junction manifests two extreme configurations with a significant on/off ratio.

In a previous investigation,[7] we developed an analytical model to explain the orientation of a $C_{20}H_{10}$ molecular bowl in a nanojunction as a function of electric field intensity, given the electronic properties (intrinsic dipole, linear polarizabilities) of the molecular units.[12] In accord with the model predictions, depending on the intensity and orientation of the electric field, dipoles induced across the surface area of the pentagonal region may become comparable or even larger than the intrinsic molecular dipole, thereby governing the orientation of the molecular component in the field.[12]

Following this same analytical model in the present work, we consider varying orientations of the active element within the CNT−[spacer]−molecule−[spacer]−CNT junctions achievable under the application of an electric field and, correspondingly, the electron transport properties through the junction. In this respect, it is first instructive to consider a series of fixed molecular orientations for the CNT−[1-ethynyl]−corannulene−[6-ethynyl]−CNT junction, where the molecule is treated as a rigid polarizable object with a single degree of freedom, the angle ϑ between the intrinsic molecular dipole P_0 and a fixed direction, as illustrated in Figure 7. This has been achieved by carrying out total-energy calculations, varying the molecular orientation from resting state ($\vartheta = 0°$) to a maximally rotated state ($\vartheta = 90°$) at fixed atomic coordinates, and correspondingly evaluating the quantum conductance (Figure 7). The quantum conductance across the series increases consistently with an increase in ϑ angle through the energy range considered, displaying a significant on/off ratio for the two extreme configurations, $G(\mathrm{Ef})_{90°}/G(\mathrm{Ef})_{0°}$, up to a factor of 20 at the Fermi energy (Figure 7).

In accord with the analytical model,[12] such a large rotation (90°) would be achievable only under ideal conditions corresponding to the application of extremely intense (unphysical) electric fields.[12] In the cases of more moderate rotations, such as ϑ = 30 and 60°, there is still, however, a significant on/off ratio in the conductance with respect to the ϑ = 0° state (e.g., a factor of 15 close to the Fermi level). According to this analysis, the maximum on/off ratio in the quantum conductance achievable under realistic conditions for this system corresponds to a factor of 15. Such a system would be quite interesting for the purpose of a molecular switch, where one seeks on/off ratios of at least 1 order of magnitude between two states.[17]

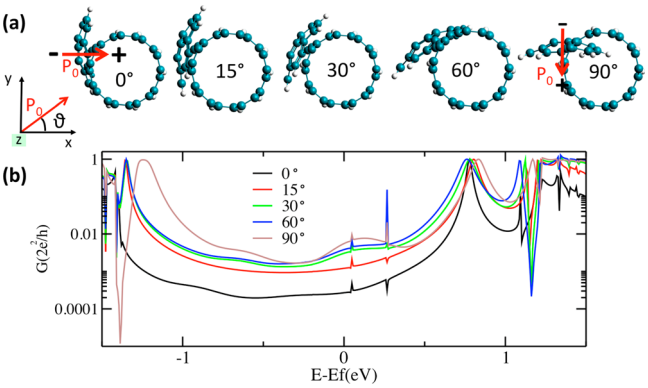

Figure 7. (a) Variation in molecular orientation in the junction in terms of the angle ϑ as defined by the intrinsic molecular dipole P_0 with the x-axis: in the two extreme cases (ϑ = 0 and 90°), the intrinsic molecular dipole P_0 is also shown. (b) Electronic conductance corresponding to the different fixed molecular orientations in the junction.

Next, the CNT−[1-ethynyl]−corannulene−[6-ethynyl]−CNT junction (Figure 1) was allowed to fully relax under the application of an electric field of 0.0055 au along the x direction and along the y direction (Figure. 8).

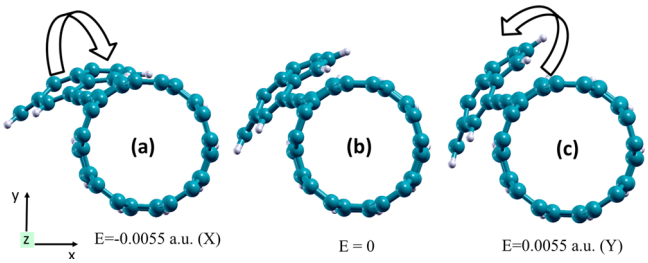

Figure 8. Relaxed structures for the CNT−[1-ethynyl]−corannulene−[6-ethynyl]−CNT molecular junctions (side views) in the absence of any electric field (b), with a field of 0.0055 au oriented along the x direction (a), with a field of 0.0055 au oriented along the y direction (c).

In agreement with the predictions of the analytical model,[12] the electric field causes the molecule to rotate with respect to the case of 0 field strength (Figure 8b) on the order of ∼30° in a clockwise direction for the field oriented along the x direction (Figure 8a). On the other hand, for the field oriented along the y direction, the molecule rotates only slightly in the counterclockwise direction (Figure 8c). However, even for the larger rotation, variations in quantum conductance compared to the 0 field case (Figure 8b) are shown to be only negligible, analogous to the difference illustrated by the static calculations between the cases of ϑ = 30 and 60° (Figure 7).

One can also investigate the extent of rotation in the field as a function of varying linker spacers. Depending on the type of linker spacer ($sp/sp^2/sp^3$) joining the molecule to the CNT

DOI: 10.1021/acs.jctc.5b00592
J. Chem. Theory Comput. XXXX, XXX, XXX−XXX

leads, the extent of molecular relaxation in the presence of the field is found to be quite different and much less than the extreme demonstrated above, ranging from essentially no rotation (sp^2 linker) to rotation on the order of 20−30° (sp and sp^3 linker). In the case of the sp^2 linker spacer, −HC═CH−, substantial rotation of the molecule in the field would require rotation about the carbon−carbon double bond, which has a relatively high energetic cost to break the π bond (~2.6 eV), substantially higher than that coming from the field strength (~0.2−0.4 eV).[12] In the case of the carbon−carbon triple bond linker spacer, the cylindrical nature of the orbital structure makes rotation of the molecule in the junction more flexible in the field (Figure 8).

Chemically Tuned Molecular Junctions: Molecule Functionalization. Variation of the morphological features (e.g., bowl depth, curvature) of functionalized $C_{20}H_{10}$[9] has been shown to modulate the intrinsic electronic character of the bowl fragments, providing an avenue for fine-tuning the electronic properties (e.g., electrical/optical band gap) with a clear structure−property relationship.[8] As such, the ability to build molecular units with tunable HOMO and LUMO energies via chemical modification should be useful for tailoring the alignment of the molecular levels with the Fermi energy of the leads for the purpose of developing chemically tuned molecular junctions. In this way, tuning the electronic conductance should be consistent and dependent on the magnitude and direction of the HOMO/LUMO shifts with respect to the Fermi energy.[17]

The first step toward modulating charge transport properties through a molecular junction via chemical modification involves active control of the electronic properties of the isolated molecules.[3] As such, initial focus was directed to the following series of isolated functionalized $C_{20}H_{10}$ systems: **1**, parent corannulene; **2**, 1,6-bispropynylcorannulene; **3**, 2,7-diethynyl-4,5-dimethylindenocorannulene; **4**, 5,10-diethynyl-2,3-difluorocorannulene; **5**, 5,10-diethynyl-1,2,3,4,6,7,8,9-octafluorocorannulene; and **6**, 5,10-diethynyl-2,4,6,8-tetrakis(trifluoromethyl)-corannulene (as shown in Figure 9). Functionalization with electron-donating vs -withdrawing groups shifts electron density through both the σ and π frame, thereby affecting the positioning of the HOMO and LUMO levels. These energy shifts in the isolated molecules can be measured, for example, as changes in the ionization potential (IP): electron-donating substituents tend to decrease the IP, whereas electron-withdrawing substituents tend to do the opposite.[3]

Theoretical predictions for HOMO, LUMO, and dipole for all isolated gas-phase molecular systems including the parent system corannulene, computed in a localized basis set framework at the PBEPBE/Def2-TZVPP level of theory, are summarized in Table 1. The corresponding values, calculated within PBE plane-wave methodology, are also shown in parentheses for the sake of comparison. The agreement between the plane-wave formulation and the localized basis set (Def2-TZVPP) description is found to be excellent. While it is well-known that DFT-based methodology using standard local or semilocal functionals may underestimate calculated IP,[39−41,3] the relative trends in the data are more reliable. Comparing trends in HOMO (LUMO) positioning across the series, one can see a relatively large and consistent lowering of HOMO (LUMO) energies, depending on the number and types of substituents, with a maximum variation of the HOMO (LUMO) position of 1.13 eV (1.37 eV) (Table 1). Comparison of HOMO (LUMO) energy between the highest and lowest

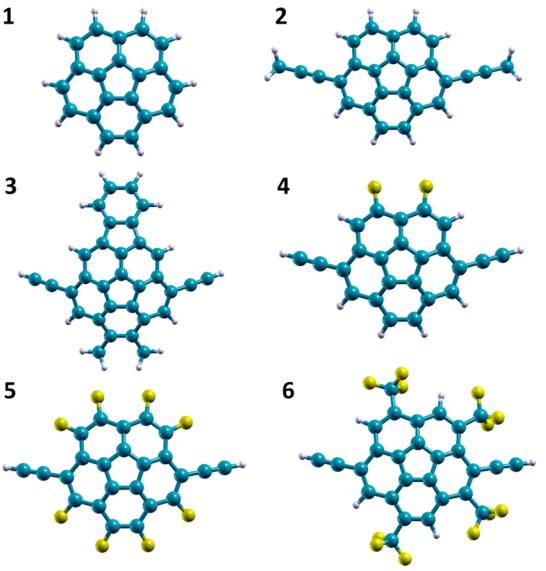

Figure 9. Molecules linked within a (5,5)-SWCNT in the molecular nanojunction systems: **1**, corannulene; **2**, 1,6-bispropynylcorannulene; **3**, 2,7-diethynyl-4,5-dimethylindenocorannulene; **4**, 5,10-diethynyl-2,3-difluorocorannulene; **5**, 5,10-diethynyl-1,2,3,4,6,7,8,9-octafluorocorannulene; and, **6**, 5,10-diethynyl-2,4,6,8-tetrakis(trifluoromethyl)-corannulene.

Table 1. PBEPBE/Def2-TZVPP (PBE Plane-Wave) Calculated Molecular Dipole Moment (D), HOMO/LUMO Energy (eV), and Bowl Depth (Å)

molecule	dipole [Debye]	HOMO [eV]	LUMO [eV]	bowl depth [Å]
1	2.09	−5.61 (−5.64)	−2.58 (−2.61)	0.90
2	2.63	−5.16 (−5.18)	−2.75 (−2.77)	0.89
3	2.93	−5.13 (−5.26)	−2.89 (−3.00)	1.08
4	2.02	−5.70 (−5.75)	−3.25 (−3.30)	0.88
5	0.39	−6.08 (−6.18)	−3.72 (−3.83)	0.80
6	2.10	−6.26 (−6.40)	−3.95 (−4.00)	0.76

dipole structure, one finds a maximum HOMO (LUMO) variation of 0.95 eV (0.83 eV) (Table 1).

Because the actual position of the frontier orbitals of the molecule as assembled in a molecular junction strongly affects the charge transport properties through the complex, it is of interest to investigate the effect of the chemical modification on the molecular-level alignment with respect to the Fermi energy of the complex in molecular junction systems. Placement of the functionalized corannulene active elements into the nanojunction using an identical sp carbon−carbon triple bond spacer linker to the (5,5)-CNT leads establishes the nanojunction systems. Here, four key nanojunction systems are considered for illustration, which, for simplicity of notation, are labeled according to the main active molecule element introduced above: **3**, **5**, **4**, and, **6**. In the final relaxed structures, all molecular components display very similar conformations to that of the pristine CNT−[1-ethynyl]−corannulene−[6-ethynyl]−CNT junction (Figure 5a), with their molecular surfaces aligned parallel to the carbon nanotube mantel. To clarify the effect of chemical functionalization on charge transport properties, a detailed look at the electronic structure and quantum conductance is necessary.

A comparison of the PDOS of the junction complex, as projected on the atomic orbitals of the functionalized molecule

DOI: 10.1021/acs.jctc.5b00592
J. Chem. Theory Comput. XXXX, XXX, XXX−XXX

component, and the DOS of the corresponding functionalized molecule in vacuum, for each of the four junctions, is shown in Figure 10. Across the series, the LUMO peaks are systematically closer to the Fermi energy, with their position varying significantly with the number and nature of substituents (e.g., **3**, 0.8 eV; **4**, 0.6 eV; **5**, 0.3 eV; **6**, 0.35 eV), than are the respective HOMO peaks (e.g., **3**, −1.2 eV; **4**, −1.4 eV; **5**, −1.5 eV; **6**, −1.5 eV), indicative of a LUMO-mediated transport mechanism.

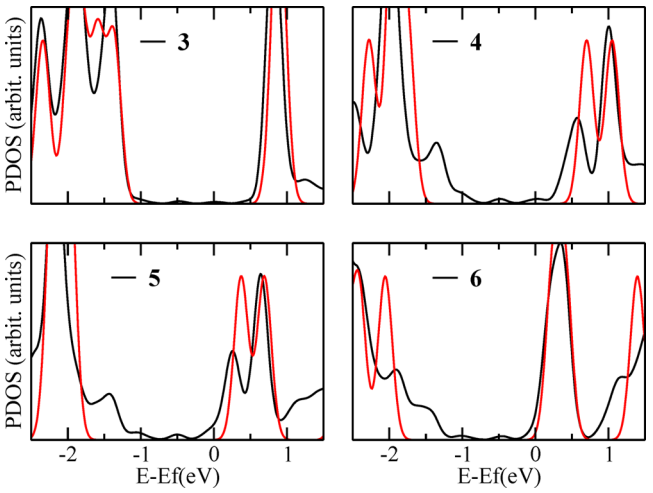

Figure 10. PDOS of the functionalized molecular unit in an assembled molecular nanojunction onto the molecule (black curve) and DOS of the gas-phase molecule (red curve).

To gauge how the tunability of the energy offset between HOMO (LUMO) and the Fermi energy due to chemical functionalization is reflected in the trends in quantum conductance through the junctions, a comparison of quantum conductance plots across the series with that of the pristine junction (**2**) (Figure 11) was made. The order of magnitude of the quantum conductance around the Fermi energy ranges between 10^{-2} and 10^{-1}, depending on chemical substitution, except for the case of **3**, where the conductance ranges up to ∼2 orders of magnitude lower. This is a special case, where the extreme rigidity of the bowl structure does not enable good mixing of molecular states with the states of the CNT to facilitate transport.

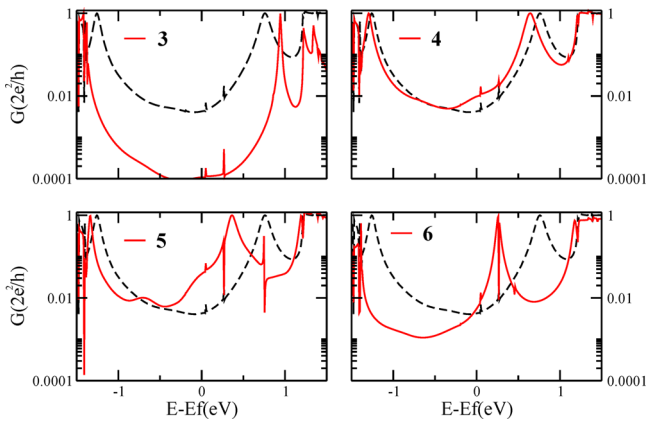

Figure 11. Quantum conductance for the functionalized molecular unit in the assembled molecular nanojunction.

In all four molecular nanojunctions considered, the two main peaks in the quantum conductance, one above and one below the Fermi level, can be ascribed to the HOMO and LUMO molecular levels, in agreement with the PDOS analysis.

Most importantly, for nanojunction systems **5** and **6**, the shift of the LUMO-related peak relative to the parent system, **2**, corresponds to a significant modulation in the quantum conductance (∼2 orders of magnitude), at 0.36 and 0.26 eV, respectively. Such tunability is of significant importance for the design of molecular junctions because it shows the potential of molecular engineering as an efficient tool for adjusting interfacial electronic structures to modulate intrinsic transport properties.

Molecular Sensor Capability. In recent years, nanostructured carbon materials have been shown to be ideally suited for sensor applications, which is attributed to their large surface-to-volume ratio that makes them sensitive to the adsorption of individual molecules.[42,43] Carbon-based materials of different dimensionality, chemically inert in their pristine form, have been shown to become highly sensitive to a large variety of molecules upon functionalization, performing quite well as detectors for small gas molecules.[43,44] In general, an effective nanosensing system should have the following components: (1) a target molecule to be detected, (2) an active element site where the target molecule may interact with the sensor, and (3) a property of the sensor that undergoes substantial modulation upon interaction with the target molecule.[18] In the present work, the nanosensing system in consideration consists of the CNT−[1-ethynyl]−$C_{20}H_{10}$−[6-ethynyl]−CNT junction, where $C_{20}H_{10}$ represents the active element site. Ideally, one would like to detect variations in the electronic conductance (property) of the junction when varying target molecules interacting with the corannulene molecule (active element site) in the junction. The target molecule may act either as an electron donor (Lewis basis) or electron acceptor (Lewis acid), as long as the interaction with $C_{20}H_{10}$ creates a fingerprint, as evidenced in the electronic conductance in terms of energy level displacement with respect to the corresponding levels in the pristine molecule. Toward this aim, the following series of molecules of varying electronegativity was considered for use as target molecules to interact with the $C_{20}H_{10}$ active element site: Br_2, ClBr, BrCl, Cl_2, and F_2 (Figure 12). One question is whether one can observe fingerprint diagnostics of either a physisorption or chemisorption process in line with their characteristic electronic properties.

The optimized PBEPBE/Def2-TZVPP gas-phase structures of the designated target molecules interacting with $C_{20}H_{10}$ are shown in Figure 12. The target molecules are approaching the $C_{20}H_{10}$ surface at varying distances, depending on the absorption mechanism involved. In the case of Br_2, BrCl, and ClBr, the final geometries are quite similar, with the target molecule pointing toward a C atom of the pentagonal ring of the active element at distances of 2.854 Å (Br_2), 2.847 Å (ClBr), and 2.832 Å (BrCl), which is compatible with a process of physisorption. When more electronegative molecules interact with the $C_{20}H_{10}$ active element, in particular F_2 and Cl_2, one sees formation of a covalent bond (1.4−1.5 Å) in a chemisorption process.

The target molecule/active element complexes in their relaxed geometry (Figure 12) were inserted into the molecular nanojunction, attached to the (5,5)-CNT with the sp CC triple bond linker spacer, to mimic the orientation of the molecule fully relaxed inside the junction (Figure 1). Focusing on these

DOI: 10.1021/acs.jctc.5b00592
J. Chem. Theory Comput. XXXX, XXX, XXX−XXX

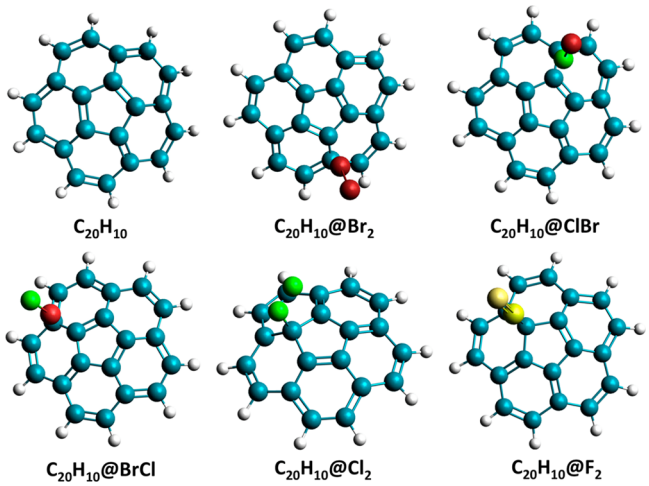

Figure 12. PBEPBE/Def2-TZVPP isolated gas-phase geometries of $C_{20}H_{10}$ and $C_{20}H_{10}$ hosting each of the target molecules.

target molecule@1,6-diethynylcorannulene junctions (molecule = Br_2, ClBr, BrCl, Cl_2, F_2), the quantum conductance was determined (Figure 13).

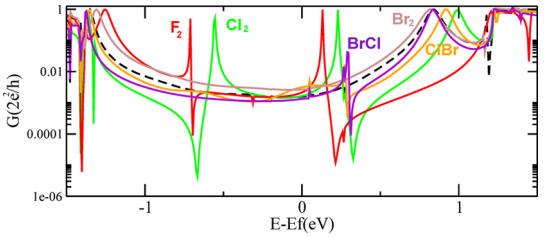

Figure 13. Quantum conductance of target molecule@1,6-diethynylcorannulene junctions, with target molecules = F_2, Cl_2, BrCl, ClBr, and Br_2. The case of a pristine junction without the presence of target molecule is also indicated (dashed black line).

Depending on the nature of the target molecule reacting with the $C_{20}H_{10}$ active element surface, one sees a series of features in the conductance plot, distinguishing the modified junctions from that of the pristine junction (dashed black line). In particular, the resulting junction indeed acts as a sensor to the type of target molecule based on its expected electronic properties and orbital mixing pattern with the active site (Figure 13).

The interaction of the small target molecules with the $C_{20}H_{10}$ active element constitutes three-orbital mixing, with the important interacting orbitals being π/π^* of the active element and σ^* of the target molecule. The degree of mixing is dependent on the level alignment between the π/π^* orbitals of the $C_{20}H_{10}$ and the σ^* orbital of the respective target molecule, the latter of which varies with the extent of electronegativity of the target molecule. At the extreme end, targets F_2 and Cl_2 have a strong interaction with the π orbitals of $C_{20}H_{10}$, resulting in a chemisorption process onto the surface of corannulene. One finds a corresponding pattern in the conductance plot, which displays two sharp peaks below and above the Fermi energy (Figure 13), indicative of states localized on the $C_{20}H_{10}$ + target molecule, as revealed by PDOS analysis (Figure 14). These peaks correspond to the interaction between the π character orbital of the 1,6-diethynylcorannulene with the σ^* (antibonding) character orbital of the F_2 (Cl_2) target molecule, also

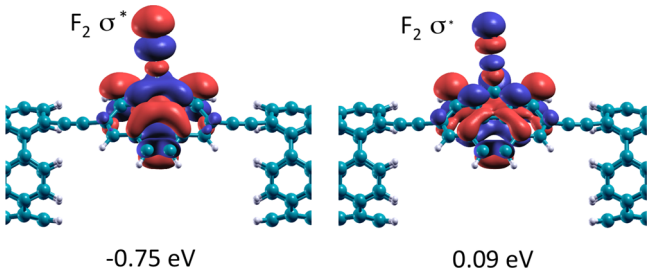

Figure 14. Orbitals corresponding to localized states coming from $C_{20}H_{10}$ HOMO and F_2 σ^*.

confirmed by PDOS. The different energy position of the F_2- and Cl_2-related peaks corresponds to the difference in energy of the corresponding σ^* orbitals for the two cases.

Across the series, as the orbital interaction modulates from weak to strong, one finds a corresponding shift in the LUMO-associated peaks toward higher energy with respect to the pristine junction in a systematic way across the series Br_2, ClBr, BrCl, Cl_2, and F_2. In the extreme case of F_2, this LUMO-associated peak actually changes shape and becomes broader.

In the intermediate cases, one finds subtle differences between ClBr and BrCl, which are distinguishable on the basis of the direction of interaction with the $C_{20}H_{10}$ surface ($C_{20}H_{10}$ ↔ Cl−Br vs $C_{20}H_{10}$ ↔ Br−Cl, respectively). In the former case, one expects a stronger interaction of the corannulene bowl with the chlorine atom such that the sensed species is actually best represented as Cl^-Br^+. However, unlike the interaction with Cl_2, ClBr does not have the same signature of chemisorption as that of F_2 and Cl_2. The signature of the strong peak below the Fermi energy is gone, and there is only a weak state localized above the Fermi energy (localized exclusively on the BrCl). In the case of BrCl, with the Br end of the diatomic interacting with the $C_{10}H_{10}$ active element, the interaction is even weaker, with a longer distance between Br and $C_{10}H_{10}$.

Finally, in the last case, Br_2, any trace of a localized state signature completely disappears. In fact, the conductance curve is quite similar to the case of the pristine junction, as the key interacting orbitals between Br_2 and $C_{10}H_{10}$ are now far apart in energy and not interacting to any detectable degree. Here, the Br_2 is clearly only physisorbed.

This series of systems constitutes a consistent set to enable investigation of the sensitivity of the methodology for the purpose of modeling nanoscale gas sensors, as detected through modification induced in the quantum conductance. Such an analysis lends itself toward the possibility of distinguishing among variations in reactivity between target molecules with the active element site in a molecular junction by looking at the signatures in the quantum conductance. As such, the results are quite promising for use in better understanding the design of chemical sensors and warrant further investigation along these lines.

Realistic Conditions. Experimentally, a molecular-scale gap within a CNT can be introduced by cutting the tube in two with a beam of oxygen atoms under ultrahigh vacuum and then exposing the tubes to a solution containing extended molecules having amine groups attached to each end, thus rejoining the two halves of the original CNT.[15] It is thought that, under these conditions, the cut ends of the CNT become terminated with carboxylic acid groups and that the reconnection involves amide-formation reactions. Unfortunately, the bridging reaction

DOI: 10.1021/acs.jctc.5b00592
J. Chem. Theory Comput. XXXX, XXX, XXX−XXX

conditions are not yet robust enough to afford junctions with atomic-level-controlled geometries.

Several theoretical studies examining prototype CNT−molecule−CNT systems have been reported, where the junction is further modified in order to account for specific experimental conditions. These studies reveal that, in addition to rigid, high-transmission junctions, a multitude of chemical factors (binding chemistries, geometries, lead details), in some cases, can have a strong impact on the transport properties. In particular, model CNT−amide−(1,4-diisocyanatobenzene)−amide−CNT transport studies have shown that CNT−molecule interface chemistry, interface geometry, CNT chirality, and molecular conformation are key areas of focus.[34,37,45−48] Results of these prototype theoretical investigations are relevant to the present work.

Ren et al.[47] investigated the impact of COOH group vs simple hydrogen chemical terminations of the CNT tubes on the electronic conductance of a CNT−1,4-diisocyanatobenzene−CNT junction. They found that chemical changes close to the junction area can have a strong influence on the channels for electron transport (shift in the resonance energies/change in the resonance widths), suggesting the potential applicability of such modifications for chemical sensing. Qian et al.[46] focused on the effect of chirality and diameter of the tubes on the molecular conductance of the same system. According to their findings, the chirality of the electrodes can affect the molecular transport, whereas other geometrical parameters, such as the diameter, the distance, and the torsion angle between the electrodes, have only negligible effects.

In contrast, Martins et al. showed[36] that, for an armchair metallic (5,5)-CNT−benzene−(5,5)-CNT molecular junction, varying the distance between the leads modifies the molecular conformation in the gap, dramatically affecting the electronic and charge transport properties, with conductance on/off ratios larger than 300. This latter study suggests the possibility of realizing a mechanically driven molecular switch.[36] CNT electrodes were also proposed for probing the conductance of a molecular switch in the case where the molecule undergoes a cis/trans conformational change when exposed to radiation. An example of such a system is azobenzene covalently attached to CNT electrodes, with substitution of the H atoms at the para-positions with NHCO groups.[49] Such modifications in topology of the contacts and/or the nanotubes' chirality show the possibility of being able to alter the low-energy conduction properties.[49]

Steric constraints are often used experimentally to minimize the possibility of multiple bridging.[15] For junctions incorporating multiple bridging molecules, there is the possibility for the bridges to interact coherently, resulting in interference effects that cause a nonlinear change in conductance with an increase in the number of bridging molecules. For example, Ashraf et al. investigated a junction incorporating three bridging diarylethenes molecules[37] and found a factor of 10^3 increase in conductance, rather than a factor of 3 increase that might be expected for three independent channels.

With these investigations in mind, in the present work we have incorporated a rather well-understood and synthetically available set of corannulene-based molecular constructs for the purpose of providing additional insight into designing new types of molecule-based devices. Throughout the set of junctions investigated here, a common lead (armchair CNT) is used together with variations in (a) active molecular element and (b) linker spacer element, in addition to examining the impact of (c) electric field and (d) external reactive element effects on the molecular element, to investigate transport properties. We have shown the importance of linker hybridization in modulating the extent of π conjugation through the junction and, ultimately, the quantum conductance. In line with previous results, strain within the linker in the designed junctions is shown to strongly affect the transport properties. A dramatic reduction in conductance is found with modifications from sp/sp^2 to sp^3 hybridization in the linker spacers due to the described double-barrier effect. Steric effects are found to impact the alignment of the molecular element with the tube structure, depending on the nature of the linker spacer and the resulting distance between the molecule and CNT leads.

Not considered in the present study is the possibility of having multiple bridging corannulene units as active elements inside the junction. This would require considerably larger diameter tubes over that of the (5,5)-CNT in order to accommodate the multiple-molecular units active elements. In such a case, as found in the literature, a nonlinear change in conductance with increasing numbers of molecular units is expected. Further modifications in chirality or diameter of the lead, while changing resonance widths and coupling strengths, is still expected to preserve the molecular origin of the main conductance peaks. The transmission spectra relates to the features of the isolated molecules, independent of tube chirality, preserving trends and transport properties.

CONCLUSIONS

Functional devices based on properties inherent in a single molecule offer considerable possibilities for use in technological applications, provided that the component molecule can take on diverse electronic functions with tuning through chemical design and synthesis. In this respect, conjugated organic molecules with delocalized π electrons have been shown to be of primary interest. In this work, the structural, electronic, and transport properties of a series of $C_{20}H_{10}$-based molecular nanojunctions have been investigated by means of first-principles DFT/electron transport techniques, enabling the transport properties to be characterized in terms of the component parts of a molecular junction. In particular, both chemical vs external perturbations of the molecular junction were identified and investigated in terms of their impact on transport phenomenon. In the former category, lead type, linker spacer type, and molecular functionality were investigated. In the latter category, the effects of an electric field and sensor molecule were investigated in terms of their influence on the molecular nanojunction for the purpose of its use as a switch technology and sensor technology, respectively. These results have implications in all categories in terms of conductance patterning and design of molecular junctions. From these results, it is clear that the special electronic properties of the corannulene molecular core, as governed by curvature and intrinsic molecular dipole, are key factors in guiding design concepts for the construction of molecular-based nanojunctions, warranting further investigation into this area.

ASSOCIATED CONTENT

Supporting Information

The Supporting Information is available free of charge on the ACS Publications website at DOI: 10.1021/acs.jctc.5b00592.

DOI: 10.1021/acs.jctc.5b00592
J. Chem. Theory Comput. XXXX, XXX, XXX−XXX

Plane wave basis tests for determination of the accuracy of electronics in the energy range of interest. Comparison of band structure of a pristine (5,5)-CNT (one single unit and 3 repeated units along the tubes's axis (principal layer)) as computed by QE vs interpolated by the atomic projections and computed electronic transmittance (PDF).

AUTHOR INFORMATION

Corresponding Author

*Tel: +41 44 635 4201; Fax: +41 44 635 6888; E-mail: kimb@oci.uzh.ch.

Funding

We gratefully acknowledge the University of Zürich, URPP LightChEC program, the National Basic Research Program of China (2015CB856500), the Qian Ren Scholar Program of China, and the Synergetic Innovation Center of Chemical Science and Engineering (Tianjin) for support of this research. A.F. thanks Italian MAE for partial support through grant no. US14GR12.

Notes

The authors declare no competing financial interest.

ACKNOWLEDGMENTS

CSCS supercomputing center is gratefully acknowledged for a grant of computer time. We are grateful to Professor Jay Siegel for helpful discussions.

REFERENCES

(1) Uoyama, H.; Goushi, K.; Shizu, K.; Nomura, H.; Adachi, C. *Nature* **2012**, *492*, 234−240.
(2) Congreve, D. l. N.; Lee, J.; Thompson, N. J.; Hontz, E.; Yost, S. R.; Reusswig, P. D.; Bahlke, M. E.; Reineke, S.; van Voorhis, T.; Baldo, M. A. *Science* **2013**, *340*, 334−337.
(3) Song, H.; Reed, M. A.; Lee, T. *Adv. Mater.* **2011**, *23*, 1583−1608.
(4) Aradhya, S. V.; Venkataraman, L. *Nat. Nanotechnol.* **2013**, *8*, 399−410.
(5) Vazquez, H.; Skouta, R.; Schneebeli, S.; Kamenetska, M.; Breslow, R.; Venkataraman, L.; Hybertsen, M. S. *Nat. Nanotechnol.* **2012**, *7*, 663−667.
(6) Guédon, C. M.; Valkenier, H.; Markussen, T.; Thygesen, K. S.; Hummelen, J. C.; van der Molen, S. J. *Nat. Nanotechnol.* **2012**, *7*, 305−309.
(7) Jia, C.; Guo, X. *Chem. Soc. Rev.* **2013**, *42*, 5642−5660.
(8) Zoppi, L.; Siegel, J. S.; Baldridge, K. K. *WIREs Comput. Mol. Sci.* **2013**, *3*, 1−12.
(9) Wu, Y.-T.; Bandera, D.; Maag, R.; Linden, A.; Baldridge, K. K.; Siegel, J. S. *J. Am. Chem. Soc.* **2008**, *130*, 10729−10739.
(10) Lovas, F. J.; McMahon, R. J.; Grabow, J.-U.; Schnell, M.; Mack, J.; Scott, L. T.; Kuczkowski, R. L. *J. Am. Chem. Soc.* **2005**, *127*, 4345−4349.
(11) Zoppi, L.; Martin-Samos, L.; Baldridge, K. K. *J. Am. Chem. Soc.* **2011**, *133*, 14002−14009.
(12) Zoppi, L.; Ferretti, A.; Baldridge, K. K. *J. Chem. Theory Comput.* **2013**, *9*, 4797−4804.
(13) Mack, J.; Vogel, P.; Jones, D.; Kaval, N.; Sutton, A. *Org. Biomol. Chem.* **2007**, *5*, 2448−2452.
(14) Bauert, T.; Zoppi, L.; Koller, G.; Garcia, A.; Baldridge, K. K.; Ernst, K.-H. *J. Phys. Chem. Lett.* **2011**, *2*, 2805−2809.
(15) Guo, X.; Small, J. P.; Klare, J. E.; Wang, Y.; Purewal, M. S.; Tam, I. W.; Hong, B. H.; Caldwell, R.; Huang, L.; Brien, S. O.; Kim, P.; Nuckolls, S. *Science* **2006**, *311*, 356−359.
(16) Feldman, A. K.; Steigerwald, M. L.; Guo, X.; Nuckolls, C. *Acc. Chem. Res.* **2008**, *41*, 1731−1741.
(17) Jia, C.; Wang, J.; Yao, C.; Cao, Y.; Zhong, Y.; Liu, Z.; Guo, X. *Angew. Chem., Int. Ed.* **2013**, *52*, 8666−8670.
(18) Mowbray, D. J.; Garca-Lastra, J. M.; Thygesen, K. S.; Rubio, A.; Jacobsen, K. W. *Phys. Status Solidi B* **2010**, *247*, 2678−2682.
(19) Perdew, J. P.; Burke, K.; Ernzerhof, M. *Phys. Rev. Lett.* **1996**, *77*, 3865−3868.
(20) Weigend, F.; Ahlrichs, R. *Phys. Chem. Chem. Phys.* **2005**, *7*, 3297−3305.
(21) Schmidt, M. W.; Baldridge, K. K.; Boatz, J. A.; Elbert, S. T.; Gordon, M. S.; Jensen, J. H.; Koseki, S.; Matsunaga, M.; Nguyen, K. A.; Su, S.; Windus, T. L.; Dupuis, M.; Montgomery, J. A. *J. Comput. Chem.* **1993**, *14*, 1347−1363.
(22) Giannozzi, P.; Baroni, S.; Bonini, N.; Calandra, M.; Car, R.; Cavazzoni, C.; Ceresoli, D.; Chiarotti, G. L.; Cococcioni, M.; Dabo, I.; Dal Corso, A.; Fabris, S.; Fratesi, G.; Gironcoli, S. d.; Gebauer, R.; Gerstmann, U.; Gougoussis, C.; Kokalj, A.; Lazzeri, M.; Martin-Samos, L.; Marzari, N.; Mauri, F.; Mazzarello, R.; Paolini, S.; Pasquarello, A.; Paulatto, L.; Sbraccia, C.; Scandolo, S.; Sclauzero, G.; Seitsonen, A. P.; Smogunov, A.; Umari, P.; Wentzcovitch, R. M. *J. Phys.: Condens. Matter* **2009**, *21*, 395502.
(23) Vanderbilt, D. *Phys. Rev. B: Condens. Matter Mater. Phys.* **1990**, *41*, 7892−7895.
(24) Calzolari, A.; Marzari, N.; Souza, I.; Nardelli, M. B. *Phys. Rev. B: Condens. Matter Mater. Phys.* **2004**, *69*, 035108.
(25) Ferretti, A.; Calzolari, A.; Bonferroni, B.; Di Felice, R. *J. Phys.: Condens. Matter* **2007**, *19*, 036215.
(26) Nardelli, M. B. *Phys. Rev. B: Condens. Matter Mater. Phys.* **1999**, *60*, 7828−7833.
(27) Meir, Y.; Wingreen, N. S. *Phys. Rev. Lett.* **1992**, *68*, 2512−2515.
(28) Agapito, L. A.; Ferretti, A.; Calzolari, A.; Curtarolo, S.; Nardelli, M. B. *Phys. Rev. B: Condens. Matter Mater. Phys.* **2013**, *88*, 165127.
(29) Landauer, R. *Philos. Mag.* **1970**, *21*, 863−867.
(30) Fisher, D. S.; Lee, P. A. *Phys. Rev. B: Condens. Matter Mater. Phys.* **1981**, *23*, 6851−6854.
(31) Ricco, B.; Azbel, M. Y. *Phys. Rev. B: Condens. Matter Mater. Phys.* **1984**, *29*, 1970−1981.
(32) Wang, S.; Zhou, L.; Zeng, Z. Y. *Phys. Rev. B: Condens. Matter Mater. Phys.* **2010**, *81*, 155438.
(33) Whalley, A. C.; Steigerwald, M. L.; Guo, X.; Nuckolls, C. *J. Am. Chem. Soc.* **2007**, *129*, 12590−12591.
(34) del Valle, M.; Gutiérrez, R.; Tejedor, C.; Cuniberti, G. *Nat. Nanotechnol.* **2007**, *2*, 176−179.
(35) Quek, S. Y.; Kamenetska, M.; Steigerwald, M. l. L.; Choi, H. J.; Louie, S. G.; Hybertsen, M. S.; Neaton, J. B.; Venkataraman, L. *Nat. Nanotechnol.* **2009**, *4*, 230−234.
(36) Martins, T. B.; Fazzio, A.; da Silva, A. J. R. *Phys. Rev. B: Condens. Matter Mater. Phys.* **2009**, *79*, 115413.
(37) Ashraf, M. K.; Bruque, N. A.; Tan, J. L.; Beran, G. J. O.; Lake, R. K. *J. Chem. Phys.* **2011**, *134*, 024524.
(38) van der Molen, S. J.; Liljeroth, P. *J. Phys.: Condens. Matter* **2010**, *22*, 133001.
(39) Cohen, A. J.; Mori-Sánchez, P.; Yang, W. *Science* **2008**, *321*, 792−794.
(40) Borghi, G.; Ferretti, A.; Nguyen, N. L.; Dabo, I.; Marzari, N. *Phys. Rev. B: Condens. Matter Mater. Phys.* **2014**, *90*, 075135.
(41) Nguyen, N. L.; Borghi, G.; Ferretti, A.; Dabo, I.; Marzari, N. *Phys. Rev. Lett.* **2015**, *114*, 166405.
(42) Reshak, A. H.; Auluck, S. *J. Appl. Phys.* **2014**, *116*, 103702.
(43) Ashori, E.; Nazari, F.; Illas, F. *Int. J. Hydrogen Energy* **2014**, *39*, 6610−6619.
(44) Mowbray, D. J.; Morgan, C.; Thygesen, K. S. *Phys. Rev. B: Condens. Matter Mater. Phys.* **2009**, *79*, 195431.
(45) Ke, S.-H.; Baranger, H. U.; Yang, W. *Phys. Rev. Lett.* **2007**, *99*, 146802.
(46) Qian, Z.; Hou, S.; Ning, J.; Li, R.; Shen, Z.; Zhao, X.; Xue, Z. *J. Chem. Phys.* **2007**, *126*, 084705.
(47) Ren, W.; Reimers, J. R.; Hush, N. S.; Zhu, Y.; Wang, J.; Guo, H. *J. Phys. Chem. C* **2007**, *111*, 3700−3704.

DOI: 10.1021/acs.jctc.5b00592
J. Chem. Theory Comput. XXXX, XXX, XXX−XXX

(48) Bruque, N. A.; Ashraf, M. K.; Beran, G. J. O.; Helander, T. R.; Lake, R. K. *Phys. Rev. B: Condens. Matter Mater. Phys.* **2009**, *80*, 155455.
(49) McNellis, E. E.; Meyer, J.; Reuter, K. *Phys. Rev. B: Condens. Matter Mater. Phys.* **2009**, *80*, 205414.

DOI: 10.1021/acs.jctc.5b00592
J. Chem. Theory Comput. XXXX, XXX, XXX−XXX